3D face recognition: An automatic strategy based on geometrical descriptors and landmarks

3D Face Recognition: an automatic strategy based on geometrical descriptors and landmarks

Enrico Vezzetti, Federica Marcolin[1], Giulia Fracastoro
Department of Management and Production Engineering
Politecnico di Torino, Italy

Abstract

In the last decades, several three-dimensional face recognition algorithms have been thought, designed, and assessed. What they have in common can be hardly said, as they differ in theoretical background, tools, and method. Here we propose a new 3D face recognition algorithm, entirely developed in Matlab®, whose framework totally comes from Differential Geometry. Firstly, 17 soft-tissue landmarks are automatically extracted relying on geometrical properties of facial shape. We made use of derivatives, coefficients of the fundamental forms, principal, mean, and Gaussian curvatures, and shape and curvedness indexes. Then, a set of geodesic and Euclidean distances, together with nose volume and ratios between geodesic and Euclidean distances, has been computed and summed in a final score, used to compare faces. The highest contribution of this work, we believe, is that its theoretical substratum is Differential Geometry with its various descriptors, which is something totally new in the field.

Keywords

Face recognition; landmark; geometry; 3D face; shape index; geodesic distance.

1 Introduction

Automated human face recognition (FR) is a non-trivial computer vision problem of considerable practical significance. It has applications including automated secured access, automatic surveillance, forensic analysis, fast retrieval of records from databases in police departments, automatic identification of patients in hospitals, checking for fraud or identity theft, and human-computer interaction (Gupta *et al.* 2010).

Literature on FR is wide and various. We have selected among the numerous contributions the most significant ones that, similarly to us, work in 3D with facial landmarks and/or possibly employ geometrical concepts to the algorithm. Gupta *et al.* (2010) proposed the new Anthroface 3D recognition algorithm after automatically detecting 10 landmarks through the support of Gaussian and mean curvatures. The algorithm compares 123 distances among a set of Euclidean and geodesic ones, performing significantly better than the well-known eigensurfaces, fishersurfaces, and Iterative Closest Point (ICP) algorithms. In many points this method is close to ours, although our landmarking procedures totally relies on geometrical background. Zhao *et al.* (2010) used their Statistical Facial Feature Model (SFAM) to perform facial Action Unit (AU) recognition. SFAM is a partial 3D face morphable model containing both global variations in landmark configuration (morphology) and local ones in

[1]Corresponding author: federica.marcolin@polito.it

terms of texture and shape around each landmark. 19 landmarks were here considered. Similarly to us, the Shape Index proposed by Koenderink and Van Doorn (1992) was computed to describe local surface properties. Also Passalis *et al.* (2011) used the Shape Index, that, together with Spin Images, was employed to support automatic landmarking. In particular, in this work a new 3D FR method is proposed that uses facial symmetry to handle pose variations. Then, an Annotated Face Model is registered and fitted to the scan. The result is a pose-invariant "geometry image". İnan and Halici (2012) proposed a 3D FR approach based on local shape descriptors to discriminate three-dimensional face scans of different individuals. Uniformly resampled 3D face data are used to generate Shape Index, curvedness, Gaussian and mean curvature values on each point of the data. Hence, they obtained bi-dimensional matrices of these descriptors representing three-dimensional geometry information.

Following Bronstein *et al.*'s (2005[a]; 2005[b]; 2006) idea that different facial expressions of the same person are isometrics, namely geodesic distances between facial reference points are equal for all emotional expressions of the same person, other researchers worked with geodesic distances as features to be compared between faces to perform FR. Berretti *et al.* (2006; 2010) proposed a 3D FR solution in presence of expression variations. 3D face models are represented by identifying the iso-surfaces originated by the set of points which are at the same geodesic distance from the nose tip. The iso-geodesics and their relationships are then described by developing through the modeling technique of three-dimensional Weighted Walkthroughs (3DWWs) capable to quantitatively represent spatial relationships between 3D surfaces. Similarly, Feng *et al.* (2007) presented a 3D face representation and recognition approach. 3D face is represented by a set of level curves of geodesic function starting from the nose tip, which is invariant under isometric transformation of the surfaces. Ouji *et al.* (2007) presented a FR approach based on dimensional surface matching. The presented matching algorithm relies on ICP that rigidly aligns facial surfaces and perfectly provides the posture of the presented probe model. Then, the similarity metric consists in computing geodesic maps on the overlapped parts of the aligned surfaces. Mpiperis *et al.* (2007) proposed a geodesic polar parameterization of the facial surface aimed at 3D FR. Face matching is performed with surface attributes defined on the geodesic plane. Li and Zhang (2007; 2009) investigated the use of multiple intrinsic geometric attributes, such as angles, geodesic distances, and curvatures, for 3D FR. Geodesic distances, and Gaussian and mean curvatures are then employed as descriptors for faces. Jahanbin *et al.* (2011) introduced a multimodal framework for FR based on local attributes calculated from range and portrait image pairs. They applied statistical feature analysis to 2D and 3D Gabor, and Euclidean and geodesic anthropometric feature sets to select the most discriminative features while discarding redundancies.

The paper is structured as follows. Section 2 deals with methodology: section 2.1 is the landmarking phase; in sections 2.2-2.4 geodesic and Euclidean distances between landmarks, and other extracted features are presented; sections 2.5 and 2.6 concern evaluation of geometrical features and final score for matching, respectively. Results are exposed in Section 3. Then, some conclusion are drawn, and, after references, an appendix is added to figure out the geometrical background of the work.

2 Method

To perform face recognition, we used different geometrical information of the face, extracted in correspondence to the position of automatically extracted landmarks. Landmarks, originally introduced by Farkas (1981), are defined as precise locations on biological forms that hold some developmental, functional, structural, or evolutionary significance (Smeets *et al.*, 2010). Among the facial features to be compared between faces, geodesic distances are the core ones. Then, in order to increase the accurateness, we added Euclidean distances, and, after having obtained nose volume, some ratios between Euclidean and geodesic distances and the behavior of the Shape Index in the *pronasal*. The entire process has been programmed in Matlab®.

The correctness of landmark localization process has been tested by the support of a plastic surgeon, who manually identified correct landmark positioning. The "true landmark" identification has been gained in both visual and contact terms by the surgeon. Once a landmark is found, the surgeon marks it with a point directly on the person's face. Afterwards, through texture mapping (Heckbert, 1986), overlapping on 3D model is performed and the Euclidean distance between the real landmark and the respective point given by the algorithm is computed.

In Figure 1 we have summarized the whole process of our FR algorithm.

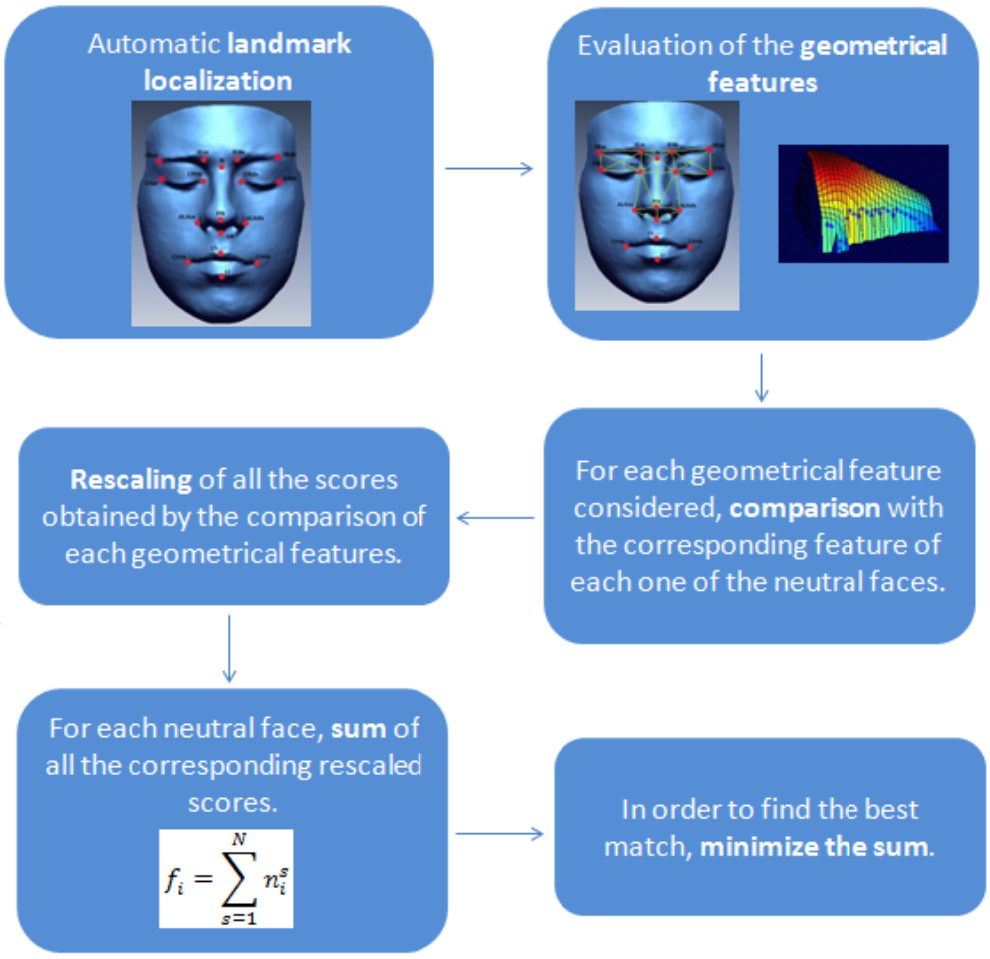

Fig. 1 The whole process of our face recognition algorithm.

2.1 Landmark extraction

The method used for automatic landmarking is explained in Vezzetti and Marcolin (2013). Considering the morphological features of the face, in order to extract the landmarks, it was necessary to employ a refining procedure that firstly identifies the region, then extracts the specific landmarks maximizing or minimizing one appropriate descriptor. Relying on the different peculiarities of the different facial regions where the landmarks are located, different combinations of the first, second and mixed derivatives (Fig. 2 and 3), the Coefficients of the Fundamental Forms E, F, G, e, f and g (Fig. 4 and 5), the curvatures K, H, k_1 and k_2 (Fig. 6 and 7) and Shape and Curvedness Indexes S and C (Fig. 8) have been employed as descriptors. The following figures (Fig. 2-8) represent these descriptor applied point-by-point to facial shells. The meaning of these geometrical descriptors is reported in the Appendix.

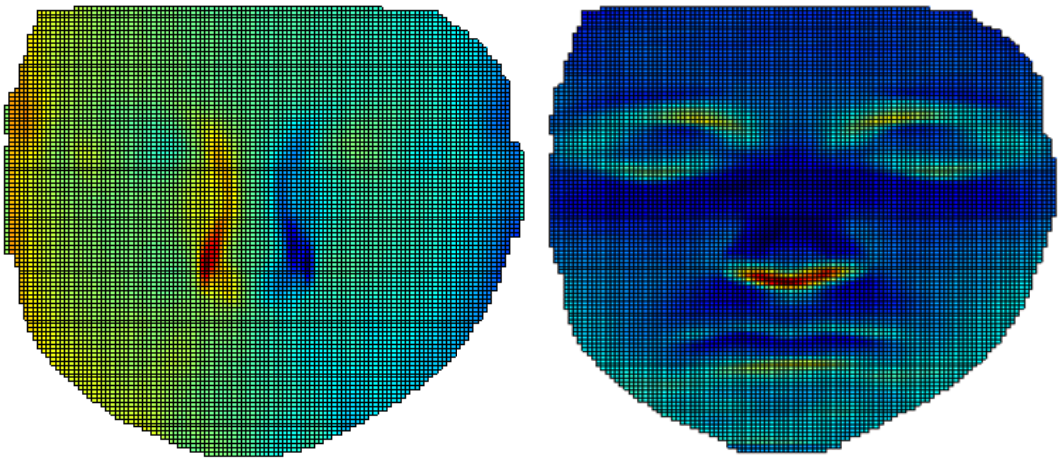

Fig. 2 The first derivatives D_x and D_y.

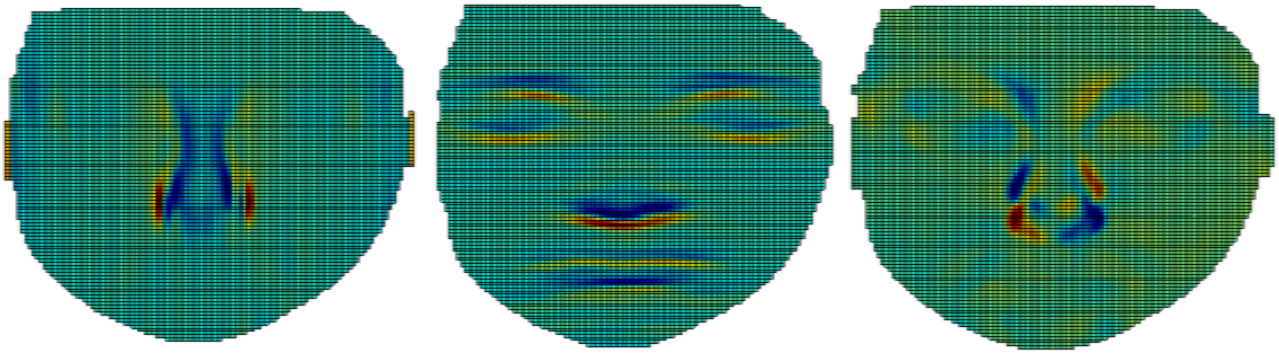

Fig. 3 The second derivatives D_{xx}, D_{yy} and D_{xy}.

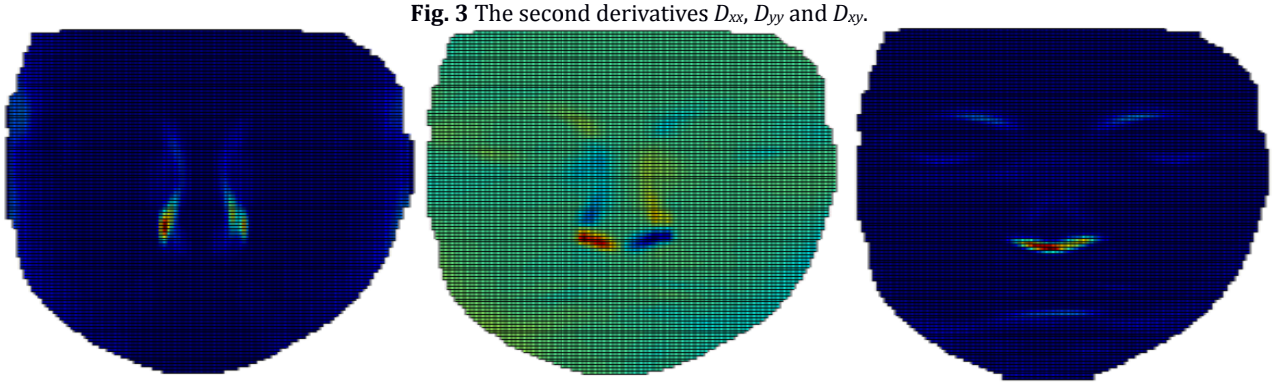

Fig. 4 The coefficients of the first fundamental form E, F and G.

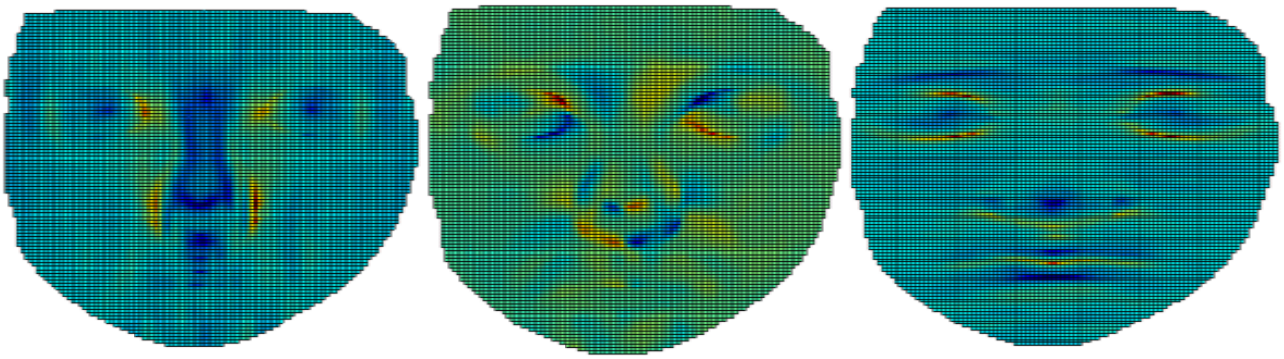

Fig. 5 The coefficients of the second fundamental form e, f and g.

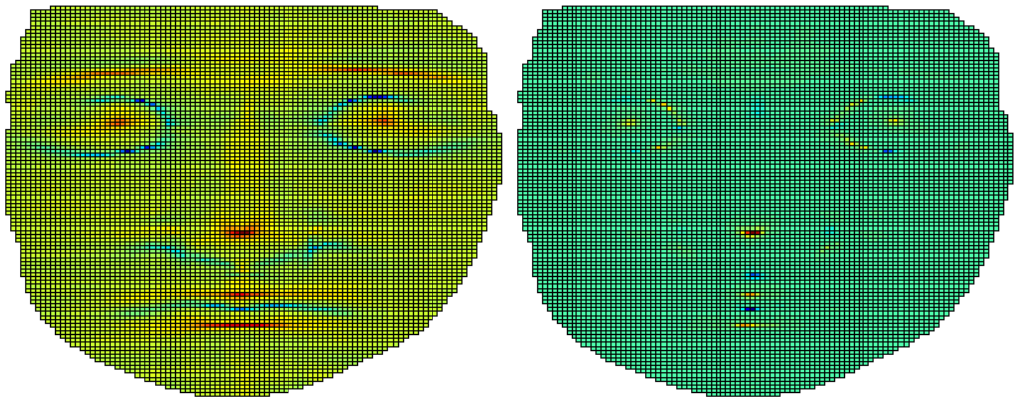

Fig. 6 The mean curvature H and the Gaussian Curvature K.

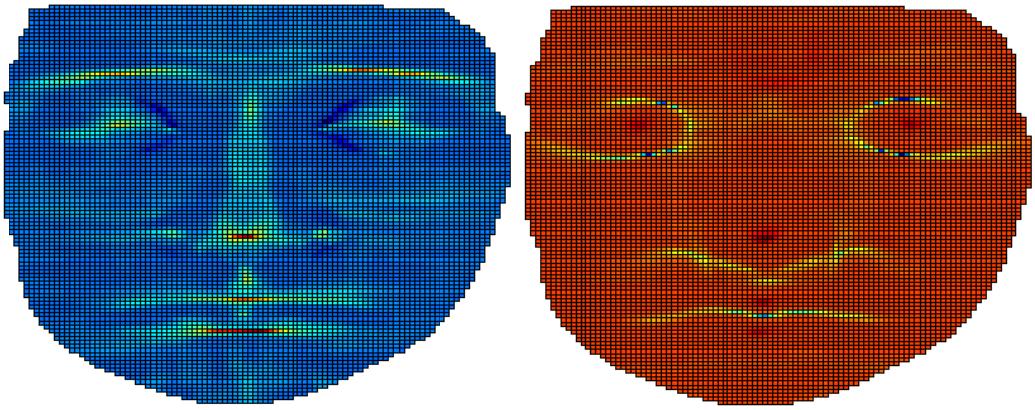

Fig. 7 The principal curvatures k_1 and k_2.

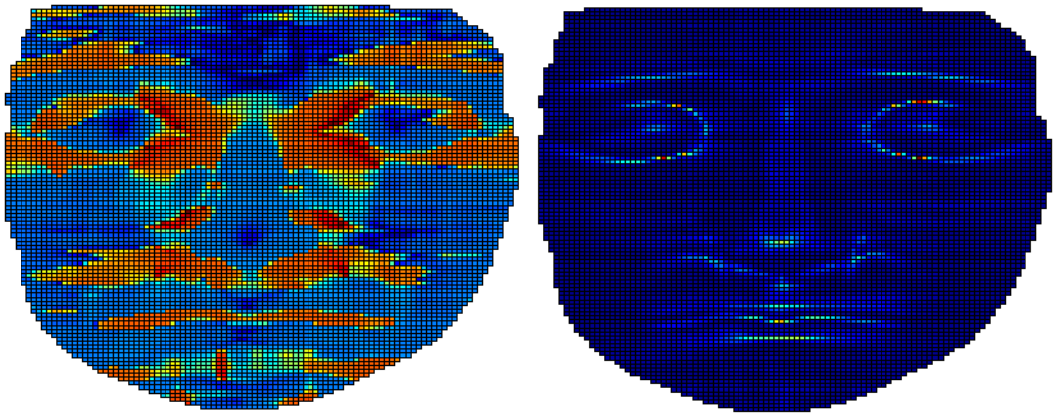

Fig. 8 The Shape and Curvedness Indexes.

The accurateness of the method explained in Vezzetti and Marcolin (2013) has been enhanced and eight other landmarks were added, reaching a total of 17 landmarks extracted (Figure 9): the *pronasal* (PN), the *subnasal* (SN), the two *alae* (ALA), the two *endocanthions* (EN), the two

exocanthions (EX), the *nasion* (N), the two *inner eyebrows* (IE), the two *outer eyebrows* (OE), the two *chelions* (CH), the *labrum superior* (LS) and the *labrum inferior* (LI).

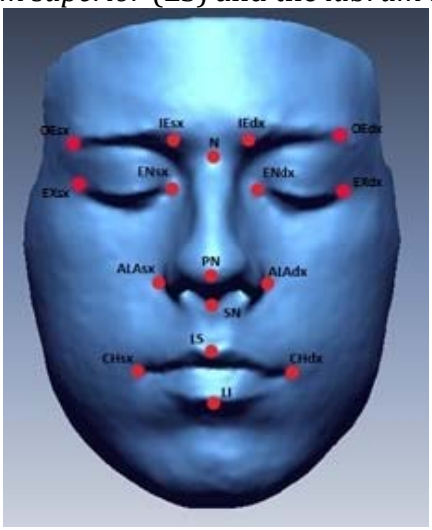

Fig. 9 The 17 landmarks used for face recognition.

Similar procedures have been employed to extract these new landmarks. For length reasons, we do not report here the whole procedure, but, in order to evaluate the accurateness of our method, we computed the distance between the landmark localized with our algorithm and the correct landmark position. In Table 1 the mean error distance and its standard deviation are shown for each landmark, the unit of measure is the millimeter.

To obtain mean errors and standard deviations, we used only a subset of our dataset, considering only the scans of 5 people, in total 35 scans (for each person we considered 7 different facial expressions).

Landmark	Mean	Standard deviation
PN	0.38	0.62
SN	0.75	0.87
ALAdx	1.56	1.25
ALAsx	1.41	1.19
ENdx	1.29	1.14
ENsx	1.82	1.35
EXdx	3.26	1.81
EXsx	3.41	1.85
N	1.04	1.02
IEdx	2.11	1.45
IEsx	2.13	1.46
OEdx	2.74	1.60
OEsx	3.40	1.84
CHdx	3.65	1.96
CHsx	2.99	1.73
LS	2.61	1.62
LI	2.06	1.43

Table 1 The error mean and standard deviation computed for the 17 landmarks.

2.2 Geodesic distances

The motivation for employing geodesic distances was that, when a surface is isometrically deformed, intrinsic properties of the surface, including geodesic distances, are preserved (Do

Carmo 1976). Bronstein *et al.* (2005-2006) proposed to model facial expressions (except when the mouth is open) as isometrics of the facial surface. Hence, algorithms based on geodesic distances are likely to be more robust to changes in facial expressions. We have computed geodesic distances between the extracted landmarks using Dijkstra's shortest path algorithm.

Among all the possible geodesic distances between the 17 extracted landmarks, we selected a subset of the most discriminatory distance features. We decided to exclude the landmarks of the mouth region, because they are too much dependent on facial expressions, e.g. mouth open or close. Moreover, we preferred the distances that do not cross the symmetry line of the face and that lie in the same region of the face, in order to construct a triangulation. Using these criteria we have detected 28 distances, represented in Figure 10.

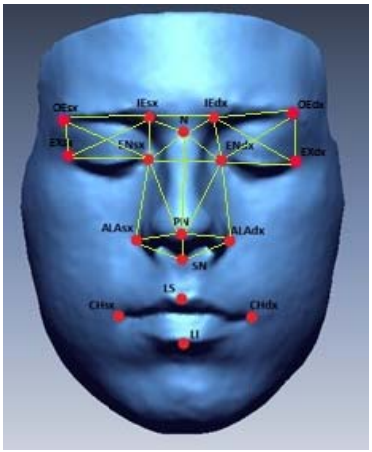

Fig. 10 The detected subset of 28 geodesic distances.

Since the landmarks are automatically extracted, the accurateness of the localization varies from one landmark and another. Moreover, the position of some landmarks is influenced by the facial expression. Therefore, we introduced two coefficients, α and β, that take into account these two aspects. The coefficient α describes the accurateness of each landmark; its values are inversely proportional to the mean error values of Table 1. In Table 2, the values of α for each landmark are shown; as can be seen they are in the range [0, 0.8].

	PN	SN	ALA	EN	EX	N	IE	OE
α	0.8	0.4	0.2	0.2	0.1	0.3	0.14	0.1

Table 2 Values of the coefficient α for each landmark (the mouth region is not considered).

The coefficient β describes how much a distance is influenced by facial expressions. In order to compute the value of β for each distance, we computed all the 28 geodesic distances using the true landmarks localized by the plastic surgeon, not the ones extracted with the algorithm. In this case we used the same subset used for the computation of mean error distances and standard deviation, i.e. considering only the scans of 5 people, each of them performing 7 facial expressions (35 scans, overall). Later, for each person of this subset, we compared the value of each distance in the shell with neutral expression with the corresponding values in the non-neutral shells. Then, for each distance, we computed the mean variation, as explained by the following formula:

$$E_i = \sum_{j=1}^{N} d_i^{(nj)} - d_i^{(j)} \vee \frac{}{N},$$

where $d_i^{(j)}$ is the value of the distance d_i in a shell of the j-th person with a non-neutral facial expression and $d_i^{(nj)}$ is the value of the distance d_i in the shell with neutral expression of the same person. Using the mean values E_i, we have classified the 28 distances in four classes. Each class corresponds to a different value of β included in the range [0, 0.5], and in each class there are seven distances. In Table 3, the different classes are shown.

Class	Value of β	Distances
1	0	PN-SN, SN-ALA, IE-OE, OE-EX
2	0.167	EN-ALA, IE-IE, EX-IE, OE-EN
3	0.33	PN-ALA, N-IE, IE-EN, EX-EN
4	0.5	PN-N, PN-EN, N-EN, EN-EN

Table 3 Classification of the distances with the corresponding β value.

After having computed α and β, we combined them in order to obtain the coefficient

$$c_i = 0.5 + \frac{(\alpha_{i1} + \alpha_{i2})}{2} + \beta_i$$

where α_{i1} and α_{i2} are the α coefficients of the two landmarks of distance d_i. The formula is defined in such a way that all the coefficients c_i range from about 0.5 to 1.5. Each c_i represent the weight for which we have to multiply the corresponding distance d_i. Then, the total difference between the geodesic distances of two faces is computed with the l_1 norm as

$$d_{geo} = \sum_{i=1}^{N} \quad c_i d_i^{(1)} - c_i d_i^{(2)} \vee$$

where N is the number of geodesic distances used and $d_i^{(1)}$, $d_i^{(2)}$ are respectively the i-th geodesic distance of face 1 and the i-th geodesic distance of face 2.

Lastly, examining the raw data for these distances, we found that for some of them the value range in all subjects was relatively similar and that the variation between subjects was not very different from the variation within subjects, making these distances of little use in recognition. So we decided to exclude these distances, obtaining a final set of 24 geodesic distances, as shown in Figure 11.

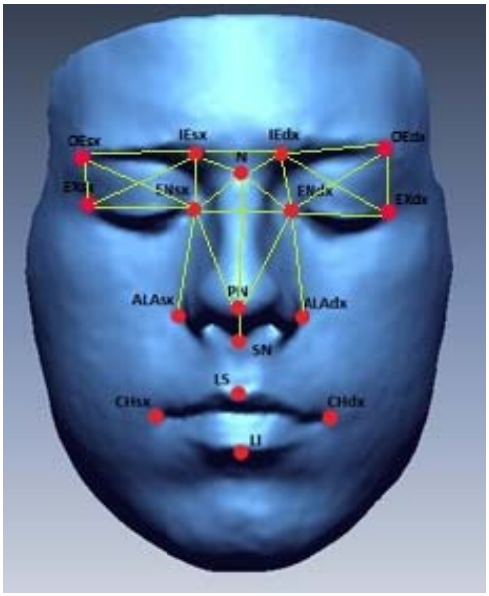

Fig. 11 The subset of 24 geodesic distances used for face recognition.

2.3 Euclidean distances

In order to improve the accurateness of the algorithm, Euclidean distances were also used. As done for the geodesic distances, we excluded the distances of the mouth region. In order to define a subset of the 28 distances presented before useful for recognition, we used the same method adopted in the previous section. We identified a subset of six distances, all quite short and in the central part of the face, as shown in Figure 12.

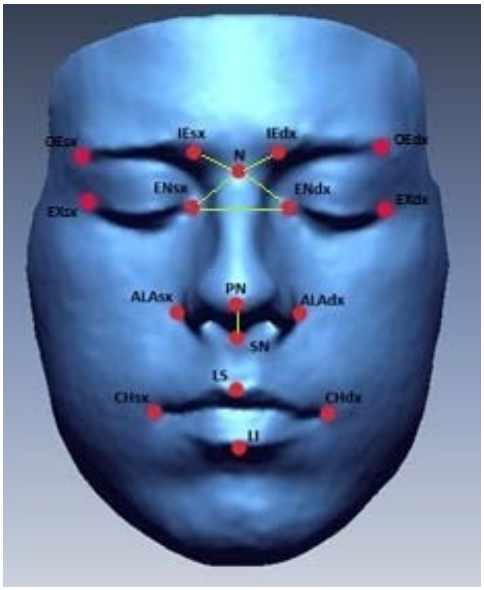

Fig. 12 The subset of 6 Euclidean distances used for face recognition.

The total difference between the Euclidean distances of two faces is computed in the same way used for the geodesic ones:

$$d_{eu} = \sum_{i=1}^{N} \quad c_i d_i^{(1)} - c_i d_i^{(2)} \text{ V},$$

where $c_i$are the coefficients calculated in the previous section, N is the number of distances used and $d_i^{(1)}$, $d_i^{(2)}$are respectively the i-th Euclidean distance of face 1 and the i-th Euclidean distance of face 2.

2.4 Other geometrical features

Geodesic and Euclidean distances cannot give a complete description of the face surface. Therefore, other geometrical information were added. Firstly, we introduced the computation of the nose volume. In this way we can have a general information about shape and dimension of the nose. In Figure 13 the volume computed is represented.

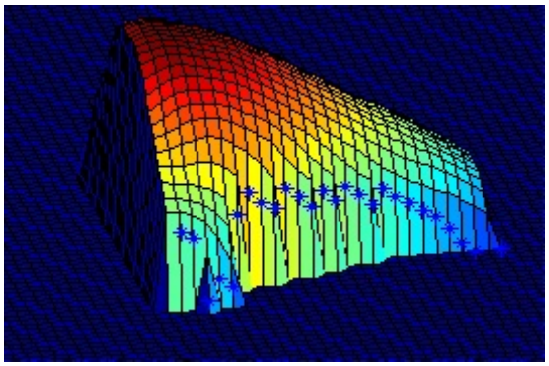

Fig. 13 The computed volume of nose.

Moreover, in order to have some information about the curvature of the nose, we introduced the following ratios between geodesic and Euclidean distances:

$$\frac{d_{PN-N}^{geo}}{d_{PN-N}^{eu}}, \quad \frac{d_{EN-EN}^{geo}}{d_{EN-EN}^{eu}}, \quad \frac{d_{ALAdx-PN}^{geo} + d_{ALAsx-PN}^{geo}}{d_{ALA-ALA}^{eu}}.$$

The last information that we used concerns the behavior of the Shape Index. We decided to compare the value of this descriptor in the *pronasal*, because is the most stable landmark. We chose the Shape Index because is the unique descriptor giving us a complete information about the shape of the surface.

For each one of the geometrical features introduced in this paragraph, the comparison between the feature values of two faces is made by computing the difference between the two values.

2.5 Evaluating the geometrical features

In order to be useful in automatic face recognition, the chosen features must ideally satisfy two criteria (Gordon 1992). (1) The first one is the repeatability; their measurement must be consistent for the same face over reasonable variation in view position and expression. (2) The second criteria is the distinctiveness; their values must vary distinctly over the range of different individuals. We evaluated these two properties for the chosen geometrical features. We computed the discriminating power of a given feature φ by considering the ratio of

between-class variance to within-class variance, where each person is considered as a class. We can express this ratio as

$$\frac{\sum_{i=1}^{c}(m_i - m)^2}{\sum_{i=1}^{c}\frac{1}{n_i}\sum_{x\in\phi_i}(x - m_i)^2},$$

where c is the number of classes (in this case, subjects), $\phi_i$is the set of feature values for class i, $n_i$is the size of ϕ_i, $m_i$is the mean of $\phi_i$and m is the total mean of the feature over all classes. Higher are the values of this criterion, more discriminating is the power. Table 4 shows the features presented above, organized from best discrimination to worst. We have evaluated these ratios using a subset of our database. The usefulness of a feature in discrimination is by nature a function of the particular dataset considered.

Feature	Between/within cluster variation
Ratio EN-EN	25.24
Geodesic distances	12.65
Volume of the nose	8.35
Euclidean distances	7.51
Shape Index	4.52
Ratio PN-N	3.84
Ratio ALA-ALA	3.41

Table 4 Ratio of between-cluster variance to within-cluster variance for each feature, ordered from best discrimination between subjects to worst.

2.6 Evaluating final match score

In order to obtain a final match score between two faces, we rescaled all the scores obtained by the comparison of each geometrical feature described above. Rescaling has been performed by multiplying each distance for a weight, so that all the distances have the same order of magnitude. The geometrical features used to perform recognition are also called 'matchers'. Then, for the final match score we used the Simple-Sum (SS), one of the most common technique of biometric fusion (Snelick 2005). So, the final score of the comparison of shell i with a neutral face is computed as

$$f_i = \sum_{s=1}^{N} n_i^s$$

where n_i^srepresents the rescaled score for matcher s and N is the total number of marchers. Then, the recognition is performed identifying the neutral shell that minimizes the score f_i.

3 Results

The algorithm was tested on a set of 217 faces that we obtained through the 3D laser scanner Minolta Vivid 910, plus a set of 27 faces taken from the public Bosphorus database. In Figure 14 three faces of this database are shown.

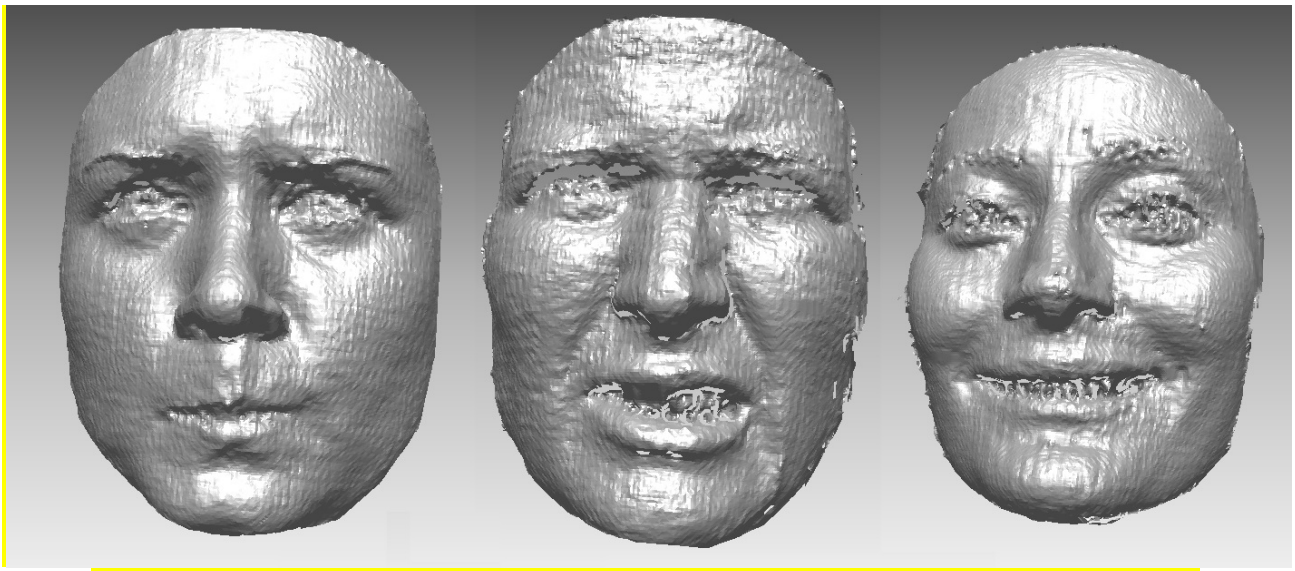

Fig. 14 Three faces of the Bosphorus dataset, performing anger, disgust, and happy expressions, respectively.

Concerning the acquired faces, 31 people have been scanned performing seven facial expressions each: serious (standard expression), anger, disgust, fear, happiness, sadness, and surprise. This choice relies on the theory of "basic emotions" of Ekman, whose studies showed that these were the six main emotional expressions (Ekman, 1970; Ekman and Keltner, 1997). The comparison process and its accurateness is obviously sensitive to which features we choose to represent the face. As we have shown above, there is wide variation in the discriminating power of our features. We tested five different sets of features. The basic set, denoted by I, includes the top 3 features of Table 3: the ratio EN-EN, the geodesic distances and the volume of the nose. The other four sets include increasing number of features added in order of discriminating power: II includes the basic set plus the Euclidean distances, III includes features from II plus the Shape Index, IV includes features from III plus the ratio PN-N, V includes features from IV plus the ratio ALA-ALA.

As previously said, we have tested our algorithm using two face sets: one with serious pose faces, 31 belonging to the faces acquired by us and 7 from the Bosphorus, that correspond to our face gallery, and one with 186 plus 20 expression-based faces of the same 31 plus 7 considered persons, respectively, that correspond to the probe set. Table 5 and Figure 15 show, for each feature set we considered, the percentage of targets for which the best match was correct.

Feature set	Accurateness
I	80.10%
II	85.92%
III	87.38%
IV	88.84%
V	90.29%

Table 5 Accurateness of the algorithm with the different feature sets.

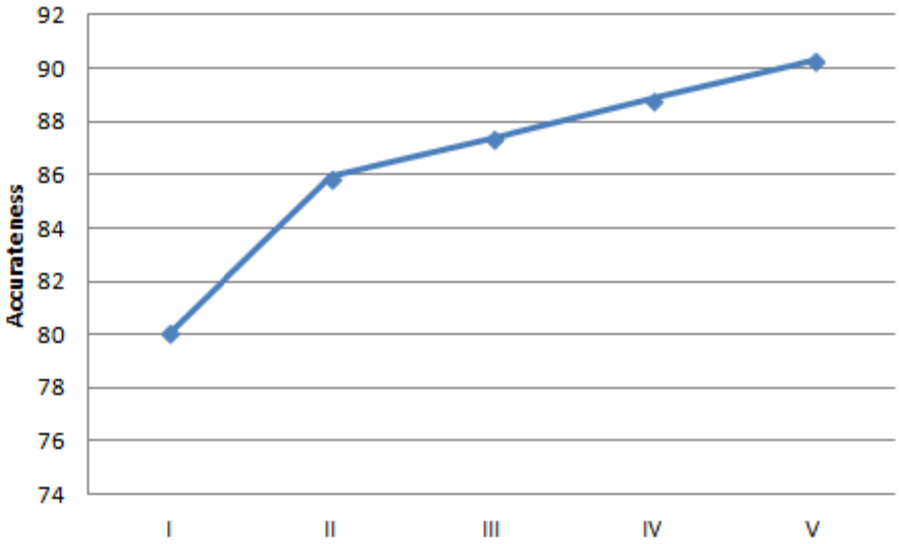

Fig. 15. Accurateness of the algorithm with the different feature sets.

The best accurateness was achieved with set V, with a percentage of 90.29%, which means 186 correct recognitions over a total of 206 recognitions performed. Furthermore, if we consider not only the best match, but the two best matches, the algorithm achieves an accurateness of 95.15%. In Table 6 it is possible to see how the accurateness changes considering from one to four best matches, we can see that, in almost all performed recognitions, the correct match is in the set of the most similar ones. In Figure 16 the Cumulative Matching Curve (CMC) from rank 1 to 10 is represented.

Best matches considered	Accurateness
1	90.29%
2	95.15%
3	96.12%
4	97.09%

Table 6 Accurateness of the algorithm considering from one to four best matches.

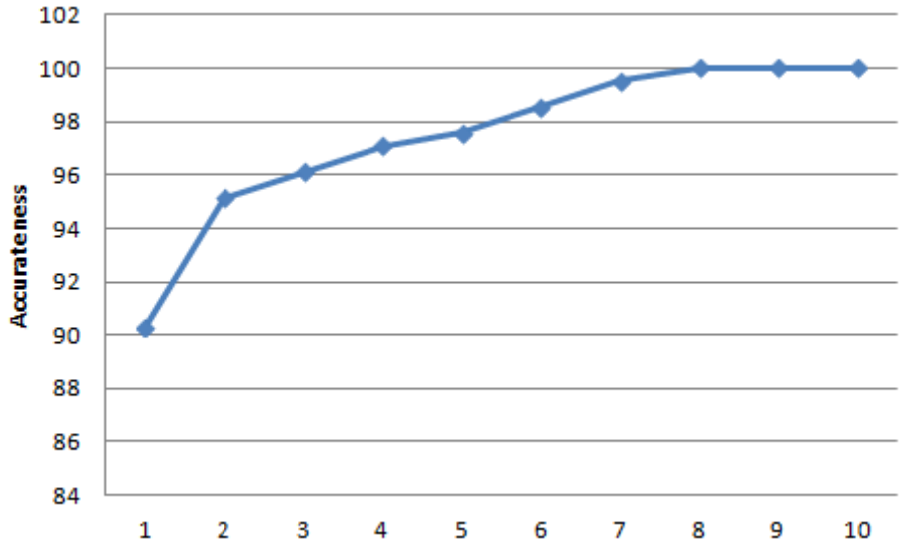

Fig. 16 The Cumulative Matching Curve (CMC) from rank 1 to 10.

4 Conclusions

This work is a totally Geometry-based 3D face recognition method. The first phase of the algorithm, entirely developed in Matlab®, consists in automatic landmarking, performed through application of Differential Geometry descriptors conditions. These descriptors are derivatives, coefficients of the fundamental forms, different types of curvatures, and Shape Index. After the landmarking phase, geodesic and Euclidean distances between landmarks, nose volume, and ratios between geodesic and Euclidean distances are computed and summed to obtain a final score to be compared between a set of 38 straight faces and a set of 206 expression-based faces of the same 38 people. Considering the best match, the accurateness of the FR algorithm is 90.29%.

Aknowledgement

The authors declare that they have no conflicts of interest to disclose.

References

Berretti, S., Del Bimbo, A., Pala, P., 2006. Description and Retrieval of 3D Face Models using iso-Geodesic Stripes. Proceedings of the 8th ACM international workshop on Multimedia information retrieval, October, 13-22.

Berretti, S., Del Bimbo, A., Pala, P., 2010. 3D Face Recognition Using Isogeodesic Stripes. IEEE Transactions on Pattern Analysis and Machine, 32(12), 2162-2177.

[a] Bronstein, A., Bronstein, M., Kimmel, R., 2005. Three-dimensional face recognition. International Journal of Computer Vision, 64(1), 5-30.

[b] Bronstein, A., Bronstein, M., Kimmel, R., 2005. Expression-Invariant Face Recognition via Spherical Embedding. IEEE International Conference on Image Processing, 3, 756-759.

Bronstein, A., Bronstein, M., Kimmel, R., 2006. Robust expression-invariant face recognition from partially missing data. Lecture Notes in Computer Science, 3953, 396-408.

Do Carmo, M. P., 1976. Differential geometry of curves and surfaces. New Jersey: Prentice-Hall.
Ekman, P., 1970. Universal Facial Expressions of Emotions. California Mental Health Research Digest, 8(4), 151-158.

Ekman, P., Keltner, D., 1997. Facial Expressions of Emotions, Lawrence Erlbaum Associates Publisher, Mahwah, New Jersey.

Farkas, L.G., 1981. Anthropometry of the Head and Face in Medicine. Elsevier North Holland, Inc, New York.

Feng, S., Krim, H., Kogan, I.A., 2007. 3D Face Recognition Using Euclidean Integral Invariants Signature. IEEE/SP 14th Workshop on Statistical Signal Processing, 156-160.

Gordon, G., 1992. Face recognition based on depth and curvature features. IEEE Computer Society Conference on Computer Vision and Pattern Recognition, 808-810.

Gupta, S., Markey, M.K., Bovik, A.C., 2010. Anthropometric 3D Face Recognition. Int J Comput Vis, 90, 331–349.

Heckbert, P.S., 1986. Survey of Texture Mapping. Computer Graphics and Applications, 6(11), 56-67.

İnan, T., Halici, U., 2012. 3-D Face Recognition With Local Shape Descriptors. IEEE Transactions on Information Forensics ans Security, 7(2), 577-587.

Jahanbin, S., Choi, H., Bovik, A.C., 2011. Passive Multimodal 2-D+3-D Face Recognition Using Gabor Features and Landmark Distances. IEEE Transactions on Information Forensics and Security, 6(4), 1287-1304.

Koenderink, J.J., van Doorn, A.J., 1992. Surface shape and curvature scales. Image and Vision Computing, 10(8), 557-564.

Li, X., Zhang, H., 2007. Adapting Geometric Attributes for Expression-Invariant 3D Face Recognition. IEEE International Conference on Shape Modeling and Applications, 21-32.

Li, X., Zhang, H., 2009. Expression-Insensitive 3D Face Recognition using Sparse Representation. IEEE Conference on Computer Vision and Pattern Recognition, 2575-2582.

Mpiperis, I., Malassiotis, S., Strintzis, M.G., 2007. 3-D Face Recognition With the Geodesic Polar Representation. IEEE Transactions on Information Forensics and Security, 2(3), 537-547.

Ouji, K., Amor, B.B., Ardabilian, M., Ghorbel, F., Chen, L., 2006. 3D Face Recognition using ICP and Geodesic Computation Coupled Approach. IEEE/ACM SITIS, Hammamet, Tunisia, 425-444.

Passalis, G., Perakis, P., Theoharis, T., Kakadiaris, I.A., 2011. Using Facial Symmetry to Handle Pose Variations in Real-World 3D Face Recognition. IEEE Transactions on Pattern Analysis and Machine Intelligence, 33(10), 1938-1951.

Smeets, D., Claes, P., Vanermeulen, D., Clement, J.G., 2010. Objective 3D face recognition: Evolution, approaches and challenges. Forensic Science International, 201, 125-132.

Snelick, R., Uludag, U., Mink, A., Indovina, M., Jain, A., 2005. Large-scale evaluation of multimodal biometric authentication using state-of-the-art systems. IEEE Transactions on Pattern Analysis and Machine Intelligence, 27(3), 450-455.

Vezzetti, E., Marcolin, F., 2013. Geometry-based 3D face morphology analysis: soft-tissue landmark formalization. Multimedia Tools and Applications, 1-35.

Zhao, X., Dellandréa, E., Chen, L., Samaras, D., 2010. AU Recognition on 3D Faces Based On An Extended Statistical Facial Feature Model. Fourth IEEE International Conference on Biometrics: Theory Applications and Systems, 1-6.

Appendix

The First and Second Fundamental Forms are used to measure distance on surfaces and are defined by

$Edu^2 + 2Fdudv + Gdv^2$,

$edu^2 + 2fdudv + gdv^2$,

respectively, where E, F, G, e, f and g are their Coefficients. Curvatures are used to measure how a regular surface x bends in R^3. If D is the differential and N is the normal plane of a surface, then the determinant of DN is the product $(-k_1)(-k_2) = k_1k_2$of the Principal Curvatures, and the trace of DN is the negative $-(k_1 + k_2)$of the sum of Principal Curvatures. In point P, the determinant of $DN_P$is the *Gaussian Curvature K* of x at P. The negative of half of the trace of DN is called the *Mean Curvature H* of x at *P.* In terms of the principal curvatures can be written

$K = k_1k_2$,

$H = \frac{k_1+k_2}{2}$.

Some definitions of these descriptors are given. These are the forms implemented in the algorithm:

$E = 1 + h_x^2$,

$F = h_xh_y$,

$G = 1 + h_y^2$,

$e = \frac{h_{xx}}{\sqrt{1+h_x^2+h_y^2}}$,

$f = \frac{-h_{xy}}{\sqrt{1+h_x^2+h_y^2}}$,

$g = \frac{-h_{yy}}{\sqrt{1+h_x^2+h_y^2}}$,

$K = \frac{h_{xx}h_{yy}-h_{xy}^2}{\left(1+h_x^2+h_y^2\right)^2}$,

$H = \frac{\left(1+h_x^2\right)h_{yy}-2h_xh_yh_{xy}+\left(1+h_y^2\right)h_{xx}}{\left(1+h_x^2+h_y^2\right)^{3/2}}$,

$k_1 = H + \sqrt{H^2 - K}$,

$k_2 = H - \sqrt{H^2 - K}$,

where h is a differentiable function $z = h(x, y)$. It is, therefore, convenient to have at hand formulas for the relevant concepts in this case. To obtain such formulas let us parametrize the surface by

$x(u, v) = \big(u, v, h(u, v)\big), \qquad (u, v) \in U,$

where $u = x$, $v = y$.

The most used descriptors are surely the Shape and Curvedness Indexes S and C, introduced by Koenderink and Van Doorn (1992):

$S = \frac{-2}{\pi} \arctan \frac{k_1 + k_2}{k_1 - k_2}, \quad S \in [-1,1], \quad k_1 \geq k_2,$

$C = \sqrt{\frac{k_1^2 + k_2^2}{2}}.$

For the role they play in the work, a little digression about their significance is needed. Their meaning is shown in Figures 17-19 and in Table 7.

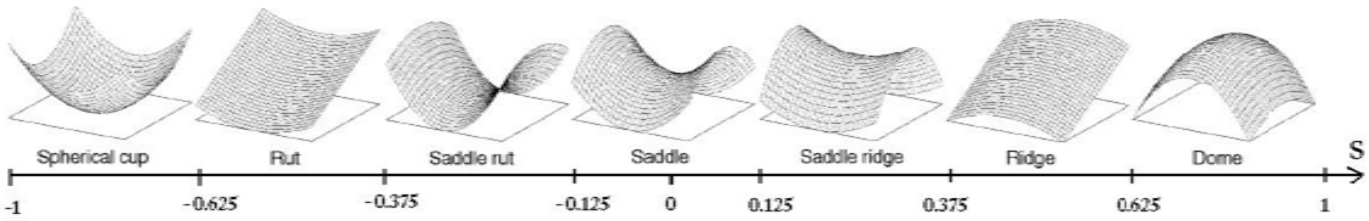

Figure 17. Illustration of Shape Index scale divided into seven categories. Different subintervals of its range [-1,1] correspond to seven geometric surfaces.

Class	***S***	**Type**	***H***	***K***
cup/pit	[-1,-0.625)	elliptical convex	+	+
rut/valley	[-0.625,-0.375)	cylindrical convex	+	0
saddle rut/saddle valley	[-0.375,-0.125)	hyperbolic convex	+	-
saddle	[-0.125,0.125)	hyperbolic symmetric	0	-
saddle ridge	[0.125,0.375)	hyperbolic concave	-	-
ridge	[0.375,0.625)	cylindrical concave	-	0
dome/peak	[0.625,1)	elliptical concave	-	+

Table 7. Topographic classes.

Figure 18. Curvedness Index scale, whose range is $(-\infty, \infty)$.

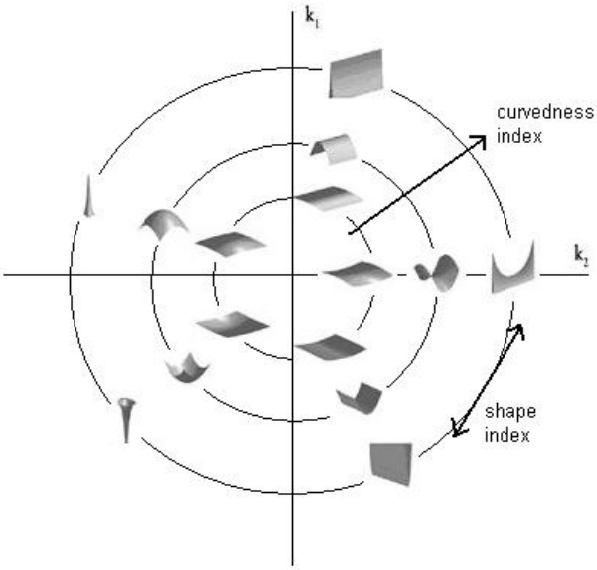

Figure 19. Indexes (S,C) are viewed as polar coordinates in the (k_1, k_2)-plane, with planar points mapped to the origin. The effects on surface structure from variations in the curvedness (radial coordinate) and Shape Index (angular coordinate) parameters of curvature, and the relation of these components to the principal curvatures (k_1 and k_2). The degree of curvature increases radially from the centre.